JOURNAL OF THERMOPHYSICS AND HEAT TRANSFER
Vol. 21, No. 3, July–September 2007

Nonlinear Thermal Model of Circular Foil Heat Flux Gauges

Brian C. Liechty,* Michael M. Clark,† Matthew R. Jones,‡
R. Scott Larson,* and Brady L. Woolford*
Brigham Young University, Provo, Utah 84602

DOI: 10.2514/1.24471

This paper presents the solution to a nonlinear model of a circular foil heat flux gauge that is exposed to a blackbody source in a vacuum environment. This is the scenario typically used to calibrate a circular foil heat flux gauge. The nonlinear model is solved using a Green's function approach. This approach results in an integral equation for the steady-state temperature profile in the gauge, which is solved using the method of successive approximations. A relationship between the incident radiative heat flux and the temperature profile is developed using this model. This relationship is compared to relationships that were derived using linear models. The first and simplest linear model neglects emission from the foil. The second linear model is obtained by linearizing the emissive power of the gauge. It is shown that these linear models only produce accurate results when the gauge design and operating conditions result in a nearly uniform foil temperature. A procedure based on the nonlinear model is proposed for optimizing the design of a circular foil heat flux gauge. A calibration procedure based on the nonlinear model is also proposed.

Nomenclature

A	=	dimensionless gauge parameter, $\varepsilon\sigma R^2 T_R^3/kt$
B	=	dimensionless irradiation, $H/\sigma T_R^4$
c	=	calibration function constants
d	=	calibration function constants
f	=	calibration functions depending on A
G	=	Green's function
H	=	irradiation, $\mathrm{W/m^2}$
h_r	=	radiation heat transfer coefficient, $\mathrm{W/m^2 \cdot K}$
I_o	=	modified Bessel function
k	=	thermal conductivity of the constantan foil, $\mathrm{W/m \cdot K}$
N_c	=	conduction-to-radiation parameter, $kt/\sigma R^2 T_R^3$
n	=	calibration function constant
R	=	radius of the constantan foil, m
r	=	radial coordinate, m
T	=	temperature, K
t	=	thickness of the constantan foil, m
γ	=	relaxation factor
$\Delta\theta$	=	dimensionless temperature difference
δ	=	Dirac delta function
ε	=	emittance
θ	=	dimensionless temperature, T/T_R
ρ	=	dimensionless radial coordinate, r/R
σ	=	Stefan–Boltzmann constant, 5.67e-8, $\mathrm{W/m^2 \cdot K^4}$

Subscripts

a	=	approximate
L	=	linear
o	=	temperature at center of heat flux gauge, K
R	=	temperature of the copper heat sink, K
1–7	=	index for calibration functions and constants

Superscript

i	=	iteration number

Introduction

HEAT flux measurements are important in the characterization, development, and optimization of systems designed for the production and use of energy. Measurement of the heat flux on a surface is challenging compared to measurement of the surface temperature. However, heat fluxes depend on thermal processes and material properties throughout the system, so a heat flux measurement provides significantly more information than a temperature measurement. In addition, heat flux measurements provide information regarding the time rate of change of temperatures within a system, so they can be extremely useful in thermal control systems.

Heat flux measurements are critical in each of the following processes and procedures: 1) monitoring and control of ovens, furnaces, kilns, and other systems used for heat-treating materials; 2) flammability testing; 3) measurement of the thermal properties of materials; 4) assessment of heating, ventilation, and air conditioning systems; 5) assessment of environmental monitoring and control systems; 6) validation of numerical thermal models of aircraft and spacecraft; and 7) validation of numerical models of combustion processes. The wide breadth and importance of these processes and procedures to the economy and to the advancement of science and technology is apparent.

An extensive review of the literature related to heat flux measurements has been written by Diller [1]. In general, heat flux gauges are classified as either calorimetric (slug) gauges in which temporal variations of the gauge temperature are measured or as diffusion gauges in which spatially resolved temperatures are measured. Operation of either type of gauge depends on a thermal model that relates the heat flux to measurable temperatures within the gauge. The thermal model is based on the geometry and thermophysical properties of the gauge, and the accuracy of the heat flux measurement depends critically on the fidelity of the model's representation of the thermal phenomena occurring within the gauge.

Circular foil heat flux gauges were first proposed by Gardon [2] in 1953, and since that time they have become a widely used diffusion-type heat flux gauge. Circular foil heat flux gauges have been studied

Presented as Paper 3277 at the 9th AIAA/ASME Joint Thermophysics and Heat Transfer Conference, San Francisco, 5–8 June 2006; received 6 April 2006; revision received 27 November 2006; accepted for publication 28 November 2006.

*Research Assistant, Department of Mechanical Engineering, 435 Crabtree Technology Building.
†Research Assistant, Department of Chemical Engineering, 350 Clyde Engineering Building.
‡Associate Professor, Department of Mechanical Engineering, 435 Crabtree Technology Building. Member AIAA.

extensively, and the effects of phenomena such as heat loss down the center wire [3,4], convective heat transfer [3,5,6], 2-D conduction in the foil [7], and the effects due to property variations have been studied [4]. The transient response of this type of gauge has also been studied [4,8]. However, the nonlinear emission from the foil has not previously been included in a thermal model of a circular foil heat flux gauge. The results presented in this paper were obtained from a rigorous thermal model that includes this nonlinear effect. These results indicate that the performance of a circular foil heat flux gauge is governed by a single dimensionless gauge parameter. The gauge parameter combines the effects of the gauge geometry, the thermophysical and radiative properties of the foil, and the temperature of the heat sink. In addition, the results of the nonlinear model clearly show the limitations of commonly used linear models. The nonlinear model also provides insight useful in optimizing the gauge design such that the impact due to the presence of the gauge is minimized. Finally, the nonlinear model can be used as the basis for a more physically realistic and, therefore, more accurate calibration procedure.

Circular Foil Heat Flux Gauges

The essential features of a copper–constantan circular foil heat flux gauge are illustrated in Fig. 1. A circular constantan foil is attached to an oxygen-free, high-conductivity (OFHC) copper heat sink. The constantan foil is usually given a diffuse, highly absorbing coating, and the gauge is designed such that heat loss from the backside of the foil is minimized. If necessary, the heat sink is actively cooled to maintain it at a constant temperature [9]. The gauge may be press fit or threaded and screwed into a wall. Copper leads are attached to the center of the foil and to the copper heat sink as shown. This configuration results in the formation of copper–constantan thermocouple junctions at the center of the foil and at the interface between the foil and the heat sink. Therefore, the voltage difference between the leads is proportional to the temperature difference between the center and the edge of the foil. A thermal model of the heat transfer processes occurring in the foil is used to develop a relationship between the measured temperature difference and the incident radiative heat flux. Originally developed as a device for measuring radiative heat fluxes [2], this type of gauge may be used to measure convective fluxes if the calibration coefficient is corrected by dividing by the absorptance of the coating [9].

Because of favorable thermophysical and thermoelectric properties, copper and constantan are the most commonly used materials in circular foil heat flux gauges. However, there are restrictions on the maximum allowable temperature at the center of the foil when this combination of materials is used [9]. In this study, a generalized design for a circular foil heat flux gauge is considered. In this generalized design, the restrictions on the maximum allowable foil temperature are lifted. Naturally, the practical implementation of such a generalized design may require the use of alternative material combinations and temperature sensors other than thermocouple junctions. Requirements for the generalized design are that a 1-D, radial temperature profile exists in the foil and that the temperatures at the center and edge of the foil be measurable by some means.

Circular foil heat flux gauges are usually calibrated by exposing them to a blackbody source in a vacuum [9]. Assuming that the irradiation is uniform over the face of the gauge, that heat losses from the back of the gauge are negligible, that temperature gradients across the thickness of the foil are negligible, that the thermal conductivity is constant, and that the surface of the gauge is diffuse and gray, the governing equation and boundary conditions for the radial temperature profile in the foil are as follows:

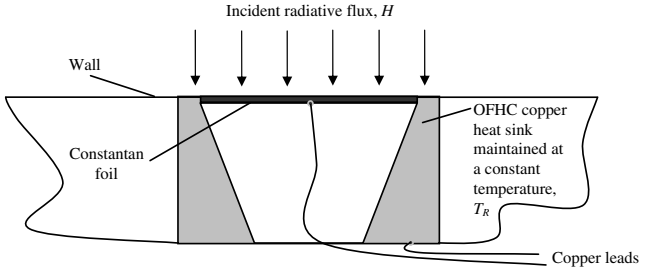

Fig. 1 Schematic diagram of a typical circular foil heat flux gauge.

$$\frac{1}{r}\frac{\mathrm{d}}{\mathrm{d}r}\left(r\frac{\mathrm{d}T}{\mathrm{d}r}\right)=\frac{\varepsilon\sigma}{kt}\left(T^4-\frac{H}{\sigma}\right) \tag{1}$$

$$\left.\frac{\mathrm{d}T}{\mathrm{d}r}\right|_{r=0}=0 \tag{2}$$

$$T(R)=T_R \tag{3}$$

To simplify the analysis and for convenience in presenting results, Eqs. (1–3) are nondimensionalized using the parameters listed in the nomenclature. The resulting nondimensional governing equation for the dimensionless temperature profile and boundary conditions are as follows:

$$\frac{1}{\rho}\frac{\mathrm{d}}{\mathrm{d}\rho}\left(\rho\frac{\mathrm{d}\theta}{\mathrm{d}\rho}\right)=A\theta^4-AB \tag{4}$$

$$\left.\frac{\mathrm{d}\theta}{\mathrm{d}\rho}\right|_{\rho=0}=0 \tag{5}$$

$$\theta(1)=1 \tag{6}$$

Note that the nondimensional radial temperature profile in the gauge is determined by the dimensionless irradiation B and the dimensionless gauge parameter A, which characterizes the combined effect of the dimensions and properties of the foil and the temperature of the heat sink. For some operating conditions, Eq. (4) can be simplified by employing additional, linearizing approximations, and relatively simple, explicit relationships between the dimensionless irradiation and the dimensionless temperature difference can be obtained. These linear relationships are presented in the following section. The following section also presents a Green's function solution to Eqs. (4–6) which does not require any linearizing approximations. The authors are unaware of any previous publication in which the nonlinear emission from the foil has been included in a thermal model of a circular foil heat flux gauge.

Approximate, Linearized, and Nonlinear Models

Approximate Solution

The simplest linear solution, referred to here as the approximate solution, is obtained by neglecting emission from the foil. Clearly, this approximation is valid when the incident radiative heat flux is large [$H/\sigma \gg T^4(r)$ or $B \gg \theta^4(\rho)$]. It will be shown that this approximation is also only valid when the foil is nearly isothermal [$T(r) \approx T_R$ or $\theta(\rho) \approx \theta(1) = 1$]. The foil will be approximately isothermal in a conduction dominated case [10]. The conduction-to-radiation parameter ($N_c = kt/\sigma R^2 T_R^3$), sometimes referred to as the Planck number [11], is commonly used to assess the importance of conduction relative to radiation. The gauge parameter is equal to the emittance divided by the conduction-to-radiation parameter ($A = \varepsilon/N_c$), so the foil will be approximately isothermal when A is small.

When emission from the foil is neglected, it can be shown that the dimensionless temperature profile is

$$\theta_a(\rho)=\frac{4+AB-AB\rho^2}{4} \tag{7}$$

and the approximate dimensionless irradiation is directly proportional to the dimensionless temperature difference between the center and edge of the foil [$\Delta\theta = \theta(0) - \theta(1) = \theta(0) - 1$].

$$B_a = \frac{4\Delta\theta}{A} \tag{8}$$

Linearized Solution

The linearized solution is obtained by linearizing the emission term:

$$\theta^4(\rho) \approx \theta^3(1)\theta(\rho) = \theta(\rho) \tag{9}$$

This approximation is valid when there are small variations in the temperature across the foil [$T(r) \approx T_R$ or $\theta(\rho) \approx 1$]. Again, the foil will be approximately isothermal when the gauge parameter is small. Substituting Eq. (9) into Eq. (4) and solving the resulting linear equation gives the following expression for the dimensionless temperature profile:

$$\theta_L(\rho) = \frac{1-B}{I_o(\sqrt{A})} I_o(\sqrt{A}\rho) + B \tag{10}$$

Based on the linearized solution, the approximate dimensionless irradiation is

$$B_L = \frac{I_o(\sqrt{A})}{I_o(\sqrt{A}) - 1}\Delta\theta + 1 \tag{11}$$

The linearized solution is equivalent to the solution obtained by Borell and Diller for calibrating circular foil heat flux gauges in convective environments [5]. If a radiation heat transfer coefficient is defined as

$$h_r = \varepsilon\sigma T_R^3 \tag{12}$$

it may be seen that the square root of the gauge parameter is equal to the dimensionless parameter introduced by Borell and Diller [5]. Borell and Diller used this dimensionless parameter to calculate a correction factor as part of a nonlinear calibration procedure for circular foil heat flux gauges that are operated in a convective environment.

Nonlinear Solution

Because the solution of the nonlinear thermal model has not been previously presented in the literature, the nonlinear solution will be presented in greater detail. The solution of the nonlinear model is obtained using a Green's function approach. The first step is to multiply the governing equation, Eq. (4), by the Green's function and integrate over the volume of the constantan foil:

$$\int_0^1 G(\rho,\rho')\frac{1}{\rho}\frac{\partial}{\partial\rho}\left(\rho\frac{\partial\theta}{\partial\rho}\right) t 2\pi\rho\,\mathrm{d}\rho = \int_0^1 G(\rho,\rho')A[\theta^4(\rho) - B] t 2\pi\rho\,\mathrm{d}\rho \tag{13}$$

Integrating the left-hand side of Eq. (13) by parts and requiring that

$$\left.\frac{\partial G}{\partial\rho}\right|_{\rho=0} = 0 \tag{14}$$

and that

$$G(1,\rho') = 0 \tag{15}$$

results in Eq. (16):

$$\int_0^1 \theta\frac{1}{\rho}\frac{\partial}{\partial\rho}\left(\rho\frac{\partial G}{\partial\rho}\right)\rho\,\mathrm{d}\rho = A\int_0^1 G(\theta^4 - B)\rho\,\mathrm{d}\rho + \left.\frac{\partial G}{\partial\rho}\right|_{\rho=1} \tag{16}$$

Next, the differential equation specifying the Green's function is obtained by requiring that

$$\frac{1}{\rho}\frac{\partial}{\partial\rho}\left(\rho\frac{\partial G}{\partial\rho}\right) = \frac{\delta(\rho-\rho')}{\rho} \tag{17}$$

Substituting Eq. (17) into Eq. (16) gives

$$\theta(\rho') = \int_0^1 \theta(\rho)\delta(\rho-\rho')\,\mathrm{d}\rho = A\int_0^1 \rho G(\rho,\rho')[\theta^4(\rho) - B]\,\mathrm{d}\rho + \left.\frac{\partial G}{\partial\rho}\right|_{\rho=1} \tag{18}$$

Therefore, once the Green's function is known, the temperature profile in the foil can be obtained from Eq. (18) without employing any linearizing approximations. The Green's function is obtained by solving Eq. (17) subject to the boundary conditions specified in Eqs. (14) and (15), and the result is given by Eq. (19):

$$G(\rho,\rho') = \begin{cases} \ell n\,\rho' & \text{for } 0 \le \rho \le \rho' \\ \ell n\,\rho & \text{for } \rho' < \rho \le 1 \end{cases} \tag{19}$$

Substituting Eq. (19) into Eq. (18) gives, after some manipulation, an integral equation specifying the dimensionless radial temperature profile in the foil:

$$\theta(\rho) = A\,\ell n\,\rho\int_0^\rho \rho'\theta^4(\rho')\,\mathrm{d}\rho' + A\int_\rho^1 \rho'\,\ell n\,\rho'\theta^4(\rho')\,\mathrm{d}\rho' + \frac{AB}{4}(1-\rho^2) + 1 \tag{20}$$

Equation (20) may be solved for the dimensionless temperature profile using the method of successive approximations [11]. In this method, an initial estimate for the temperature profile is substituted into the right-hand side of Eq. (20) and the integrals are evaluated numerically. Use of an underrelaxation technique was required for this iterative procedure to remain stable, so subsequent estimates of the dimensionless temperature profile were obtained from a weighted sum of the previous estimate and the right-hand side of Eq. (20):

$$\theta^i(\rho) = (1-\gamma)\theta^{i-1}(\rho) + \gamma\left[A\,\ell n\,\rho\int_0^\rho \rho'(\theta^{i-1})^4\,\mathrm{d}\rho' + A\int_\rho^1 \rho'\,\ell n\,\rho'(\theta^{i-1})^4\,\mathrm{d}\rho' + \frac{AB}{4}(1-\rho^2) + 1\right] \tag{21}$$

The linearized solution given by Eq. (10) may be used as the initial estimate for the dimensionless temperature profile. Typically, the relaxation factor was between 10^{-4} and 10^{-1}, and smaller relaxation factors were required when the dimensionless irradiation was large. Faster convergence may be obtained if a more sophisticated relaxation method is used in which the relaxation factor is increased in proportion to the number of iterations. Once a converged solution for the temperature profile is obtained, the dimensionless irradiation may be calculated using Eq. (22):

$$B = \frac{4\Delta\theta}{A} - 4\int_0^1 \rho[\theta(\rho)]^4\,\ell n\,\rho\,\mathrm{d}\rho \tag{22}$$

An interesting observation is made by combining Eq. (8) with Eq. (22):

$$B_a = B + 4\int_0^1 \rho[\theta(\rho)]^4\,\ell n\,\rho\,\mathrm{d}\rho \tag{23}$$

Because the integral term on the right-hand side of Eq. (23) is always negative, the approximate dimensionless irradiation is biased to values less than the actual dimensionless irradiation. The integral on the right-hand side of Eq. (23) is negligible when $\theta(\rho) \approx 1$, but is significant otherwise. ASTM International recommends calibrating circular foil heat flux gauges using a linear relationship with a zero intercept [9]. The model used to relate the incident heat flux to the voltage output by the gauge in the ASTM standard is equivalent to the approximate model, and Eq. (23) shows that the approximate model is a poor representation of the actual system when there is an appreciable temperature gradient across the foil.

A second observation may be made by considering the limiting case of a uniform foil temperature [$\theta(\rho) \rightarrow 1$ and $\Delta\theta \rightarrow 0$]. Steady-state operation under these conditions requires that absorbed irradiation equal the emitted radiative flux or that the dimensionless irradiation is equal to one. Note that values given by Eq. (22) for B and by Eq. (11) for B_L converge to the correct limit of one. However, the value given by Eq. (8) for B_a converges to an incorrect value of zero under these conditions.

The bias error and the incorrect physical behavior inherent in the approximate model highlight the need to use a more physically correct model as a basis for the calibration procedure of circular foil heat flux gauges.

Temperature Profiles Calculated Using the Linear Models

Figure 2 shows representative temperature profiles obtained using the approximate and linearized models compared with the temperature profiles obtained using the nonlinear model for specified values of the dimensionless irradiation and the gauge parameter. In Fig. 2a, the temperature profiles based on the approximate and linearized models agree well with the temperature profiles predicted by the nonlinear model for small values of the gauge parameter and large values of the dimensionless irradiation. Figure 2b shows that the temperature profiles calculated using the approximate and linearized models are significantly higher than the profile based on the nonlinear model for moderate values of A and B.

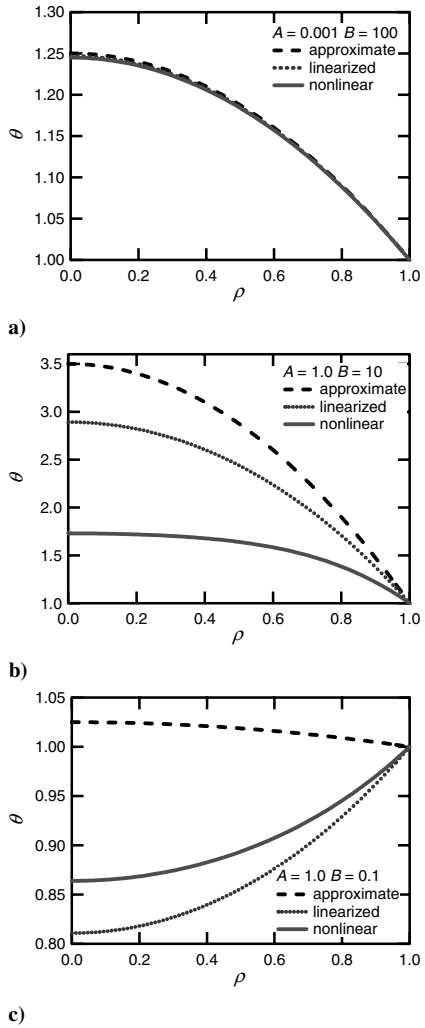

Fig. 2 Representative foil temperature profiles. Profiles obtained using the approximate and linearized models are compared with profiles based on the nonlinear model for specific values of the dimensionless gauge parameter and dimensionless irradiation.

Under normal operating conditions in which the foil is at elevated temperatures, the linearized emissive power is always less than the actual emissive power of the foil. Therefore, the temperature profile based on the linearized model will exceed that of the nonlinear model to compensate under these conditions. A more accurate linearized model would use an average foil temperature instead of the heat sink temperature when linearizing the emissive power. However, this would require an iterative solution procedure because the average foil temperature is initially unknown.

Although circular foil heat flux gauges were originally developed to measure intense radiative fluxes, use of these gauges to measure relatively weak radiative fluxes has been suggested.[§] Temperature profiles calculated for a case in which the dimensionless irradiation is less than one are shown in Fig. 2c. When $B < 1$, conservation of energy requires that foil temperatures be less than the heat sink temperature, and under these conditions, heat will be conducted from the copper ring into the foil. Because the approximate model does not include emission by the gauge, which is not negligible under these conditions, the temperature profile obtained using the approximate model is physically unrealistic. The linearized model includes emission by the foil, but the temperature profile predicted using the linear model is still inaccurate. Under these operating conditions, the linearized emissive power is greater than the actual emissive power, so the linearized temperature profile must be less than the nonlinear temperature profile to compensate.

Measurement of the Incident Radiative Flux Using the Linear Models

Because the purpose of the gauge is to measure the incident radiative flux, the ability of the approximate and linearized models to predict the dimensionless irradiation under a wide variety of conditions was investigated. In this study, the dimensionless temperature difference between the center and edge of the foil was calculated using the nonlinear model for specified values of the gauge parameter and the dimensionless irradiation. These simulated "measurements" were input into Eqs. (8) and (11), and the dimensionless irradiation was calculated using both the approximate and linearized models.

Plots of approximate dimensionless irradiation B_a and of the linearized dimensionless irradiation B_L vs the actual dimensionless irradiation B for a wide rage of values of the gauge parameter are shown in Fig. 3. As expected, Fig. 3a shows that B_a is always biased to values less than B. In addition, accurate results are only obtained when the gauge parameter is small and when the dimensionless irradiation is large. Figure 3b shows that the linearized model produces accurate results for a wider range of B values than does the approximate model, but again only when the gauge parameter is small.

An alternative presentation of this data is shown in Fig. 4, in which contour plots of the error in the "measured" dimensionless radiation are plotted for both the approximate and linearized models.

The results for the approximate model are shown in Fig. 4a. Error levels less than 10% are obtained for small gauge parameters and for a dimensionless irradiation greater than ten. When the dimensionless irradiation is less than ten, neglecting the emission term is a poor approximation, and the underlying assumption in the approximate model is no longer valid. As expected, errors associated with the approximate model increase rapidly as the dimensionless irradiation decreases. In fact, $\Delta\theta$ becomes negative for $B < 1$ as discussed in the preceding section, and the approximate model predicts a negative incident radiative flux under these conditions.

As shown in Fig. 4b, error levels less than 10% are obtained using the linearized model over a wide range of dimensionless irradiation values. However, the error associated with the linearized model increases rapidly if the value of the gauge parameter exceeds 0.1. Another interesting observation is that as the value of the dimensionless irradiation approaches 1, the error in B_L is less than

[§]Data available online at www.vatell.com/thermogage.htm [retrieved 7 March 2006].

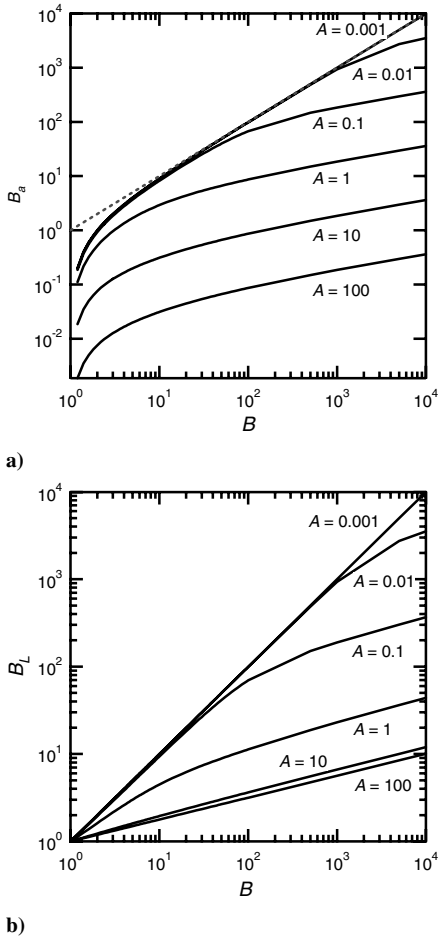

Fig. 3 Comparison of the dimensionless irradiation calculated using a) the approximate model and b) the linearized model with the dimensionless irradiation input to the nonlinear model for a range of values of the gauge parameter.

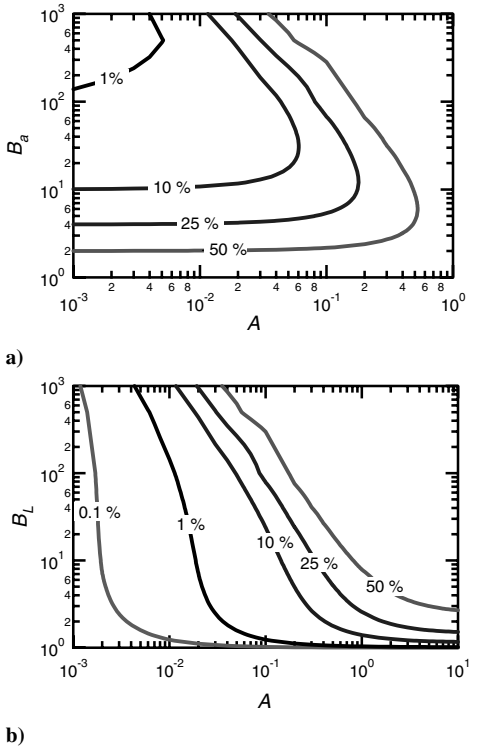

Fig. 4 Contour plots of the error in the "measured" dimensionless irradiation as a function of the gauge parameter. a) Results for the approximate model; b) results for the linearized model.

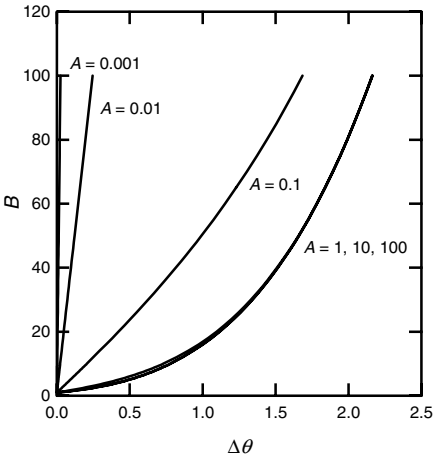

Fig. 5 Dimensionless irradiation as a function of the dimensionless temperature difference. Predictions are based on the nonlinear model.

0.1% for all values of the gauge parameter. This result is due to the fact that at $B = 1$, the emissive power of the foil is equal to the irradiation, and the foil must have a uniform temperature T_R. Under these conditions, the linearized solution is exact, and results based on the linearized solution are identical to results based on the nonlinear model.

These results show that the linearized model gives accurate results for a wide range of values of the dimensionless irradiation as long as the dimensionless gauge parameter is less than approximately 0.1. Because the gauge parameter is proportional to T_R^3, restricting the gauge parameter to values less than 0.1 limits the allowable values for the temperature of the heat sink. A limitation on the allowable heat sink temperature necessitates that the gauge be water cooled when it is mounted in a high temperature surface. Maintaining the temperature of the heat sink below that of the wall perturbs the wall temperature profile, and the resulting localized low temperature region surrounding the gauge increases the flux incident on the gauge above that which would be incident on the wall in the absence of the gauge.

An additional disadvantage of requiring small values for the gauge parameter can be seen by considering Fig. 5. Dimensionless foil temperature profiles were calculated using Eq. (21) for values of the dimensionless irradiation in the range of $1 \leq B \leq 100$ and values of the gauge parameter in the range of $0.001 \leq A \leq 100$. The dimensionless irradiation is plotted as a function of the dimensionless temperature difference between the center and the edge of the foil for various values of the gauge parameter in Fig. 5. The linear relationship between B and $\Delta\theta$ for small values of the gauge parameter is clearly evident in this figure. The steep slope of these lines indicates that the measured dimensionless irradiation is extremely sensitive to the dimensionless temperature difference under these operating conditions. This high sensitivity is concerning because a slight error in the measured temperature difference will be greatly magnified and result in a significant error in the measurement of the incident radiative flux. A precision thermocouple can measure temperatures within a tolerance of 0.5 K [12]. Introducing this level of error into measurements of T_R and the temperature at the center of the gauge, T_o, will result in significant error in the heat flux measurement, as illustrated by the following example. Assuming a 0.5 K error in these two measurements, the error in $\Delta\theta$ is ± 0.001 under typical operating conditions ($300 < T_R < 500$ K and $1.1T_R < T_o < 2.0T_R$). At $A = 0.001$, the slope of the curve in Fig. 5 is approximately 4000. Thus, with an error in $\Delta\theta$ of 0.001, the measured dimensionless flux B can be determined within a tolerance of ± 4. Thus, the incident flux H must be at least 40 times larger than σT_R^4 to obtain a heat flux measurement with an uncertainty less than 10%. At $A \geq 1$, the dimensionless flux is independent of A and all curves in the figure are identical. The slope of the curves for $A \geq 1$ in Fig. 5 changes with $\Delta\theta$, resulting in variable sensitivity over the plotted range of $\Delta\theta$. However, the slope at all points along the higher A value curve is significantly shallower than the $A = 0.001$ curve. At

$A \geq 1$, the error in measuring B is only ± 0.006 at B ≈ 1 and a maximum error of ± 0.1 occurs at B ≈ 100.

Optimizing the Design and Operation of Circular Foil Heat Flux Gauges

Use of the approximate or linearized model as a basis for calibrating a circular foil heat flux gauge is desirable because these models predict a simple linear relationship between the desired parameter, the dimensionless irradiation, and the most conveniently measured parameter, the dimensionless temperature difference between the center and the edge of the foil. However, the results presented in the preceding section demonstrate that there is a limited range of operating conditions where these linear models are valid. Restrictions on the magnitude of the gauge parameter are particularly limiting in that they do not allow the heat sink temperature to be matched to the wall temperature in many applications. In addition, requiring the gauge parameter to be small produces gauges that are sensitive to noise in the measurement of the temperature difference between the center and edge of the foil. Therefore, the development of operating procedures based on the nonlinear model that allows larger values of the gauge parameter would be beneficial. However, Eq. (22) shows that the nonlinear model predicts that the dimensionless irradiation depends on the dimensionless temperature profile in the gauge as well as the dimensionless temperature difference.

The lack of a simple relationship between the dimensionless irradiation and the dimensionless temperature difference is clearly evident in Fig. 5. However, knowledge of the entire dimensionless temperature distribution can be eliminated by curve fitting the data and using a suitable calibration technique. The functional form of the data in Fig. 5 is

$$\left.\begin{aligned} B &= f_3(A)\Delta\theta^3 + f_2(A)\Delta\theta^2 + f_1(A)\Delta\theta + 1 \quad \text{for } 0.1 \leq A < 1 \\ f_1(A) &= c_1 A^n \\ f_2(A) &= c_2 A^2 - c_3 A + c_4 \\ f_3(A) &= c_5 A^2 + c_6 A + c_7 \\ B &= d_1\theta^3 + d_2\theta^2 + d_3\theta + 1 \quad \text{for } 1 \leq A \leq 100 \end{aligned}\right\} \tag{24}$$

At larger values of the dimensionless gauge parameter ($A \geq 1$), the dimensionless flux is independent of A and the data fit well to a cubic polynomial. However, as the gauge parameter diminishes, the dependence of B on A becomes large and the cubic function must morph into a straight line. This behavior results in a more complex functional form for $B(\Delta\theta, A)$. Note that Eq. (24) was developed for the range of $1 \leq B \leq 100$ and $0.1 \leq A \leq 100$ and the data may diverge from Eq. (24) outside this range. When the gauge parameter is less than 0.1, the linearized model can be used for a wide range of B.

Equation (24) contains a set of undetermined parameters, which must be determined by experimental calibration of the gauge. The calibration can be accomplished by altering the radiant source and/or the dimensionless gauge parameter (i.e., by adjusting the heat sink temperature). The accuracy of the gauge can then be determined by using known radiant sources other than those used to determine the set of calibration parameters in a blind test.

The following example, based on numerical simulations, illustrates how the proposed calibration procedure could be performed. The data for this numerical experiment were generated using the nonlinear model, Eq. (21). Four values of A (0.1, 1, 10, 100) and 76 values of B within the range $1 \leq B \leq 100$ were chosen. Each combination of these values was input to Eq. (21), and 304 values of $\Delta\theta$ were calculated. The undetermined coefficients in Eq. (24) were then determined using a least-squares method. Values for all parameters are listed in Table 1. A test for accuracy of the calibration curve was conducted by randomly selecting values of the dimensionless irradiation within the range of 1 to 500 and values of the gauge parameter within the range of 0.1 and 100. None of the randomly chosen values for A and B matched those used to determine the calibration coefficients. Equation (21) was used to generate foil temperature profiles for each combination of A and B. The resulting dimensionless temperature difference was used in Eq. (24) to predict the dimensionless irradiation, and these values were compared to the actual values. The results are listed in Table 2. The calibration curve is more accurate when the gauge parameter is greater than approximately 1 and when the dimensionless irradiation is within the range of 10 to 100. Within these ranges, the error is typically less than 5%. It is noted that the errors listed in Table 2 are confidences for the curve fit to the nonlinear model. The low errors, however, illustrate that the functional form of the calibration model [Eq. (24)] is adequate over a large range of operating parameters.

Table 1 Calibration parameters for Eq. (24) obtained from a computer simulation

Constant	Value
n	−0.6715
c_1	8.916
c_2	19.20
c_3	−24.22
c_4	2.914
c_5	−11.69
c_6	17.14
c_7	3.277
d_1	8.200
d_2	0.6043
d_3	5.994

Table 2 Percent error in the dimensionless irradiation predicted by the calibration curve, Eq. (24), for randomly generated values of A and B

	A			
B	0.255	0.787	8.28	82.7
3.70	10.8%	3.39%	4.98%	5.09%
4.53	10.7%	1.03%	3.12%	3.19%
10.2	8.05%	5.02%	1.00%	0.990%
25.7	5.51%	2.96%	0.630%	0.590%
41.4	5.49%	1.24%	0.190%	0.090%
69.1	4.44%	0.22%	0.180%	0.300%
233.0	7.40%	1.45%	3.40%	3.14%
367.0	13.4%	3.30%	6.24%	5.91%
373.0	13.6%	3.38%	6.35%	6.02%

The results of this study suggest the following procedure for optimizing both the design and operation of a circular foil heat flux gauge:

1) Choose the heat sink temperature to be equal to the temperature of the wall in which the gauge will be mounted. This will minimize the disturbance due to the presence of the gauge and help insure that the measured heat flux closely represents the heat flux that would exist if the gauge was not present.

2) Adjust the radius, thickness, and emittance of the foil such that the gauge parameter falls within the range of 0.1 to 100. The results presented in Fig. 5 indicate that the sensitivity of the gauge will be optimal for these conditions.

3) Consistent with current practice, calibrate the gauge using radiant sources [9]. However, rather than fitting the data to a simple linear relationship with a zero intercept, the data should be fit to nonlinear relationships between the dimensionless irradiation and the dimensionless temperature difference, Eq. (24). In general, the coefficients for the $\Delta\theta$ terms in the calibration curves are functions of the gauge parameter.

Conclusions

A solution to a nonlinear model of a circular foil heat flux gauge that is exposed to a blackbody source in a vacuum environment has been developed. Expressing the model in dimensionless form reveals the governing dimensionless parameter, the gauge parameter, which characterizes the combined effect of the dimensions and properties of

the foil and the temperature of the heat sink. The gauge parameter is equal to the emittance of the gauge divided by the conduction-to-radiation parameter.

The nonlinear model is solved using a Green's function approach. This approach results in an integral equation for the steady-state temperature profile in the gauge. A relationship between the dimensionless irradiation and the dimensionless temperature profile in the foil is developed using this nonlinear model. This relationship is used to assess the accuracy of two linear models over wide ranges of values of the gauge parameter and of the dimensionless irradiation. The approximate model was found to be accurate to within approximately 10% for $A < 0.01$ and $10 < B < 500$. The linearized model was accurate to within approximately 10% for $A < 0.1$ and $1 < B < 500$.

When the gauge parameter is greater than 0.1, the nonlinear model must be used. The ability to obtain accurate results when the gauge parameter is greater than 0.1 is significant in that it allows the heat sink temperature to be matched to the wall temperature. Perturbations in the wall temperature profile will be minimized when the heat sink is in thermal equilibrium with the wall, and the measured heat flux will be more representative of the heat flux that would exist in the absence of the gauge.

A procedure for optimizing the design and calibrating a circular foil heat flux gauge that is based on the nonlinear model is proposed. Sample calculations based on the proposed procedure indicate that errors will be less than approximately 5% for $1 \leq A \leq 100$ and $10 < B < 100$. These results are based on numerical experiments, and efforts to experimentally validate these results are underway.

References

[1] Diller, T. E., "Advances in Heat Flux Measurement," *Advances in Heat Transfer*, edited by J. P. Hartnett, T. F. Irvine, Jr., and Y. I. Cho, Vol. 23, Academic Press, Boston, 1993, pp. 279–368.

[2] Gardon, R., "An Instrument for the Direct Measurement of Intense Thermal Radiation," *Review of Scientific Instruments*, Vol. 24, No. 5, 1953, pp. 366–370.

[3] Ash, R. L., and Wright, R. E., "Design Considerations for Gardon Heat Flux Sensors," AIAA Paper 71-470, 1971.

[4] Malone, E. W., "Design and Calibration of Thin-Foil Heat Flux Sensors," *ISA Transactions*, Vol. 7, No. 3, 1968, pp. 175–180.

[5] Borell, G. J., and Diller, T. E., "A Convection Calibration Method for Local Heat Flux Gages," *Journal of Heat Transfer*, Vol. 109, No. 1, 1987, pp. 83–88.

[6] Kuo, C. H., and Kulkarni, A. K., "Analysis of Heat Flux Measurements by Circular Foil Gages in a Mixed Convection/Radiation Environment," *Journal of Heat Transfer*, Vol. 113, No. 4, 1991, pp. 1037–1040.

[7] Kirchoff, R. H., "Response of Finite-Thickness Gardon Heat-Flux Sensors," *Journal of Heat Transfer*, Vol. 94, No. 2, 1972, pp. 244–245.

[8] Keltner, N. R., and Wildin, M. W., "Transient Response of Circular Foil Heat Flux Gages to Radiative Fluxes," *Review of Scientific Instruments*, Vol. 46, No. 9, 1975, pp. 1161–1166.

[9] Anon., "Standard Test Method for Measuring Heat Flux Using a Copper-Constantan Circular Foil, Heat-Flux Transducer," ASTM International Paper E 511-01, 2001.

[10] Özisik, M. N., *Radiative Transfer and Interactions with Conduction and Convection*, Werbel & Peck, New York, 1973, Chap. 6.

[11] Modest, M. F., *Radiative Heat Transfer*, 2nd ed., Academic Press, Amsterdam, 2003, Chap. 8.

[12] Holman, J. P., *Experimental Methods for Engineers*, 5th ed., McGraw–Hill, New York, 1989, Chap. 8.